Bioactive Site-Specifically Modified Proteins for 4D Patterning of Gel Biomaterials

Jared A. Shadish[1], Gabrielle M. Benuska[2], Cole A. DeForest*[1,3-5]

Affiliations:

[1]Department of Chemical Engineering, University of Washington, Seattle, WA 98195, USA.

[2]Department of Biochemistry, University of Washington, Seattle, WA 98195, USA.

[3]Department of Bioengineering, University of Washington, Seattle, WA 98105, USA.

[4]Institute of Stem Cell & Regenerative Medicine, University of Washington, Seattle, WA 98109, USA.

[5]Molecular Engineering & Sciences Institute, University of Washington, Seattle, WA 98195, USA.

*Correspondence to: profcole@uw.edu

Abstract:

Protein-modified biomaterials can be used to modulate cellular function in 3D. However, as dynamic heterogeneous control over complex cell physiology continues to be sought, strategies that permit reversible and user-defined tethering of fragile proteins to materials remain in great need. Here, we introduce a modular and robust semisynthetic approach to reversibly pattern cell-laden hydrogels with site-specifically modified proteins. Exploiting a versatile sortase-mediated transpeptidation, we generate a diverse library of homogenous, singly functionalized proteins with bioorthogonal reactive handles for biomaterial modification. We demonstrate the photoreversible immobilization of fluorescent proteins, enzymes, and growth factors to gels with excellent spatiotemporal resolution while retaining native protein bioactivity. Dynamic regulation of proliferation, intracellular mitogen-activated protein kinase signaling, and subcellularly resolved receptor endocytosis is accomplished through localized epidermal growth factor presentation. Our method broadly permits modification and patterning of a wide range of proteins, providing newfound avenues to probe and direct advanced cellular fates in 4D.

Main text:

The extracellular matrix (ECM) directs cell function through a complex choreography of biomacromolecular interactions in a tissue-dependent manner. Far from static, this hierarchical milieu of biochemical and biophysical cues presented within the native cellular niche is both spatially complex and constantly changing[1–3]. As these pericellular reconfigurations are vital for tissue morphogenesis, disease regulation, and healing, *in vitro* culture platforms that recapitulate such dynamic environmental phenomena would be invaluable for fundamental studies in cell biology, as well as in the engineering of functional human tissue[4,5]. Polymer-based hydrogels represent one such emerging and highly attractive class of *in vitro* cell culture constructs that offer promise for dynamic 3D biological studies[6–8]. Their high water content, tissue-like elasticity, and facile transport of nutrients and waste render them ideal mimics of the cell's ECM, while their optical clarity permits imaging of cell function to be performed non-destructively[9–11]. Gel materials can be produced under mild, cytocompatible conditions that enable live-cell encapsulation and are readily formulated to contain user-defined chemical functionalities, mechanical properties, and degradability[12–14]. Through appropriately developed chemistries, such niche characteristics can be modified on-demand to probe and direct cell fate in response to variable microenvironmental cues similar to those comprising the native ECM[15–17].

To emulate dynamic ECM biochemical heterogeneity *in vitro*, significant effort has been dedicated towards the creation of an expansive library of chemical strategies for hydrogel alteration. Preliminary efforts in this regard have largely focused on the exploitation of photochemical techniques to pattern bioactive small molecules and peptides spatially within synthetic hydrogel culture systems[18–23]. While such approaches have proven successful in

directing relatively simple cellular functions (such as adhesion and spreading), the ability to regulate more complex and dynamic decisions of fate using full-length proteins remains of prime interest[24–27]. Though proteins represent a powerful tool in the quest to govern cell physiology, their fragility necessitates that careful consideration be given to the chemistries employed as well as the precise site of protein modification for material tethering to ensure sustained stability and activity[28].

Installation of reactive groups onto proteins required for biomaterial decoration has been performed almost exclusively through non-specific reactions with thiols and primary amines on endogenous cysteine and lysine residues[29]. As these amino acids are not uniquely present on native proteins, bioconjugation of this type occurs randomly and stochastically to yield a heterogeneous collection of differently modified species. Such uncontrolled functionalization often leads to protein unfolding, loss of activity, and supraphysiologic doses required to elicit cellular response. Coupled with batch-to-batch variability and ambiguous extents of modification, reproducibility problems dramatically hinder laboratory and clinical translation of these ill-defined samples. Generalizable strategies to create homogeneous protein populations that can be used to modify a wide variety of biomaterial platforms while retaining native levels of bioactivity remain an open challenge.

Chemoenzymatic strategies have gained recent popularity for their unique ability to modify proteins in a manner that is site-specific, selective, and quantitative, thereby permitting the introduction of reactive chemical handles at defined locations[30–34]. We identified the sortase-mediated transpeptidation modification strategy[34,35] as one that could permit installation of

functional handles compatible with virtually any chemistry used for biomaterial formation or modification, including photoreactions that have previously proven beneficial for 4D biomaterial decoration. Sortase A, a calcium-assisted transpeptidase from *Staphylococcus aureus*, recognizes the sorting signal "LPXTG" (where X is any amino acid) and forms an acyl-enzyme intermediate with the sorting signal's threonine residue, simultaneously displacing other C-terminal amino acids[36]. The resultant thioester intermediate can be nucleophilically displaced by reaction with the N-terminal amine of a polyglycine probe, thereby conjugating a synthetic peptide onto the C-terminus while regenerating the sortase A enzyme. Critically, the polyglycine compound may contain non-natural functionality, providing a route to "sortag" a wide variety of bioorthogonal and reactive moieties site-specifically onto proteins of interest. We hypothesized that these selectively monofunctionalized species would retain significantly higher activity than those generated through random modification, and that sortagged species would likely open the door to precisely regulate advanced cellular functions throughout biomaterials that have proven inaccessible *via* conventional strategies.

To facilitate one-step protein biofunctionalization and purification, we implemented sortagging through the recently developed Sortase-Tag Enhanced Protein Ligation (STEPL) technique[37] (Figure 1a). In STEPL, the protein of interest, sorting sequence LPETG, $(GGS)_5$ flexible linker, sortase A, and a 6xHis-Tag are fused into a single protein construct which is recombinantly expressed. The flexible $(GGS)_5$ linker allows intramolecular sortagging through the encoded LPETG motif and the fused sortase domain. The sortase-LPETG intermediate is displaced by the addition of calcium and a customizable probe with an N-terminal polyglycine moiety, ligating the protein of interest to the engineered peptide while simultaneously separating it from the

remaining 6xHis-functionalized sortase A. This step can be performed during immobilized metal ion affinity chromatography, where sortase A remains bound to the nickel-nitrilotriacetic acid (Ni-NTA) column, allowing for site-specific labeling and purification of proteins in a single step.

To highlight the versatility of sortase for protein modification and to generate a library of functional biomacromolecules for hydrogel modification, we constructed STEPL expression systems for six proteins spanning three distinct classes: fluorescent [Enhanced Green Fluorescent Protein (EGFP), mCherry, and mCerulean], enzymatic [β-lactamase (bla)], and growth factor [epidermal growth factor (EGF) and fibroblast growth factor (FGF)] (Supplementary Methods). As protein functional modification by sortase is defined by engineered peptide identity, we synthesized and exploited five distinct polyglycine probes (Figure 1b, Supplementary Methods) each with different reactive handles (azides, aromatic aldehydes, nitrobenzyl moieties). These bioorthogonal handles enable proteins to be conjugated to materials formed by a variety of common gel formation click chemistries (such as azide/alkyne, oxime, and hydrazine conjugation), as well as dictate how functionalized proteins interface with materials over time. With these six expression vectors and five sortaggable probes in hand, STEPL was utilized to generate all 30 possible protein-peptide conjugates (Supplementary Methods and Supplementary Table 1). Whole-protein mass spectrometry and gel shift assays revealed exceptionally high protein purity and quantitative functionalization in all cases (Figure 1c-h, Supplementary Figures 1-2 and Methods), indicating efficient generation of a diverse collection of singly modified proteins for gel patterning. This represents the largest library of sortagged proteins created for any application to date.

Having successfully generated site-specifically modified proteins bearing functionality required for gel decoration, we sought to compare the effects of sortagged modification versus stochastic N-hydroxysuccinimide (NHS) ester labeling of solvent-accessible amines, the most commonly employed method to modify proteins, using a representative protein from each class (Figure 2a-i). EGFP activity was evaluated directly through fluorescence measurements. Activity of bla was determined through a standard colorimetric assay involving hydrolysis of the chromogenic cephalosporin nitrocefin. EGF activity was quantified using HeLa cells expressing EKAREV, a Förster resonance energy transfer (FRET) reporter for mitogen-activated protein kinase (MAPK) signaling[38]. In all cases, azide-modified proteins sortagged with H-GGGGDDK(N_3)-NH_2 exhibited activity that was statistically indistinguishable from that of the native species. In contrast, protein bioactivity decreased significantly when azide tagging occurred through conventional NHS ester labeling involving 2,5-dioxopyrrolidin-1-yl 4-azidobutanoate (N_3-OSu). We note that large molar excesses of the NHS-activated compound relative to the protein of interest are required for even modest levels of protein labeling (Supplementary Figure 3), as NHS ester hydrolysis represents the dominant reaction pathway when this chemistry is performed in aqueous systems[39]. We also note that individual proteins tolerate different amounts of random modification, as higher excesses of the NHS species were required to diminish EGFP fluorescence (a protein that has been engineered for its stable structure) than bla enzyme activity. Taken together, these experiments demonstrate that sortagging allows for the creation of modified protein conjugates with higher purity and bioactivity than their NHS-modified counterparts.

Having observed that sortagging outperformed NHS chemistry when introducing reactive azides onto EGFP, bla, and EGF, we set out to quantify the bioactivity of all 30 protein-peptide library members (Figure 2j-o). Similar to EGFP, mCherry and mCerulean activity was evaluated directly through fluorescence measurements. FGF and EGF activity were determined based on their ability to stimulate cell proliferation, quantified by increased dsDNA synthesis and content. In total, the overwhelming majority (27/30) of modified proteins exhibit bioactivity that is statistically indistinguishable from the unmodified species. Moreover, the least active conjugate (bla-*o*NB-CHO, based on the kinetically perfect bla enzyme that had previously proven highly sensitive to modification) retained 76 ± 4% of its native bioactivity. We expect the ability to singly modify functionally diverse bioactive proteins with several different reactive handles, each of which influences how they form the basis of and interact with materials, to be hugely enabling for a variety of biological applications. Additionally, the relative ease and lack of specialized equipment required for protein expression/purification, coupled with the commercial availability of sortaggable peptides containing functional handles [including azides, alkynes, (meth)acrylates, thiols, aldehydes, maleimides, allyl sulfides], render these strategies practically accessible to non-specialists.

After verifying that sortagged proteins retained native bioactivity, we sought to demonstrate their controlled incorporation within biomaterials. Exploiting strategies previously introduced by our laboratory[27], we utilized model hydrogels formed through strain-promoted azide-alkyne cycloaddition (SPAAC) between a four-arm poly(ethylene glycol) (PEG) tetrabicyclononyne and a linear PEG diazide (Supplementary Methods). Reaction kinetics and bioorthogonality permit encapsulation of live cells with high viability, while the bioinert PEG provides a non-fouling

"blank slate" for subsequent decoration with proteins. The optical clarity of these materials renders them useful for photochemical modification with biomolecules, as well as for microscopy-based assays of encapsulated cell fate.

A cytocompatible photomediated oxime ligation[27,40] was exploited to immobilize site-specifically modified proteins within hydrogels containing a 2-(2-nitrophenyl)propyloxycarbonyl (NPPOC)-photocaged alkoxyamine with spatiotemporal control (Figure 3ab). Upon mild near-UV irradiation (λ = 365 nm), NPPOC is cleaved, liberating the reactive alkoxyamine and permitting localized condensation with gel-swollen aromatic aldehyde-modified proteins to form a stable oxime linkage. Removal of unbound proteins by diffusion yields patterned gel substrates defined by user-selected light exposure locations and parameters. Gel patterning was performed with EGFP sortagged with H-GGGGDDK(CHO)-NH_2 (EGFP-CHO), whereby immobilized protein fluorescence permitted visualization and quantification. Traditional photolithographic techniques were utilized to control patterning of mask-defined shapes throughout gel thickness (Figure 3c), and to generate continuous gradients that followed a dose-dependent response predicted by NPPOC photocleavage kinetics (Figure 3df, Supplementary Figure 4). EGFP-CHO was immobilized within hydrogels with excellent 3D control through multiphoton laser-scanning lithography, whereby programmed laser rastering within the gel material dictated protein tethering location and concentration (Figure 3e, Supplementary Figure 5). These experiments represent the first demonstration of 3D patterned covalent immobilization of a site-specifically modified protein within a material.

After having demonstrated the ability to immobilize sortagged proteins within biomaterials with excellent 3D control, we shifted our efforts towards the patterned photorelease of such species from gels (Figure 3g). For this, we exploited an *ortho*-nitrobenzyl ester (*o*NB) moiety[22,41] that undergoes rapid photoscission in response to cytocompatible near-UV light (λ = 365 nm) (Figure 3h). mCherry sortagged with H-GGGGDDK(*o*NB-N_3)-NH_2 (mCherry-*o*NB-N_3) was tethered uniformly throughout materials during SPAAC-based gelation. After directed light exposure, released protein was diffused from the gel prior to sample imaging and quantification through fluorescent confocal microscopy. Mask-based photolithographic techniques were again exploited to control mCherry-*o*NB-N_3 removal and concentration throughout full gel thickness in a predictable and dose-dependent manner (Figure 3ijl, Supplementary Figures 6-7). Multiphoton lithography afforded excellent 3D patterning at user-specified regions within gels (Figure 3k, Supplementary Figure 8). These results represent the first photorelease of a site-specifically modified protein from a 2D or 3D material. In addition to controlling the location of immobilized proteins that persist within a gel, the fully defined and homogenous protein population photoreleased from the material may have significant implications for controlled drug delivery.

Sortase's versatility in introducing diverse functional handles onto different proteins of interest enables protein-patterned materials of unprecedented complexity to be photoevolved in 4D. To demonstrate dynamic material patterning, we selected three differentially modified and spectrally separated fluorescent proteins from our library of sortagged species. Gels containing the NPPOC-caged alkoxyamine were uniformly functionalized with mCherry-*o*NB-N_3. Upon directed light exposure, mCherry photorelease was performed in concert with photomediated ligation of an aldehyde-tagged protein (either mCerulean-CHO or EGFP-*o*NB-CHO) to create

interconnected biochemical patterns. The photorelease/oxime ligation sequence was repeated, enabling a third protein (either EGFP-*o*NB-CHO or mCerulean-CHO) to be immobilized (Figure 4a). This approach was utilized to create an Escher-inspired tessellation of fish/bird shapes through masked lithography (Figure 4b-e, Supplementary Figure 9), as well as a 3D schematic depiction of a cell binding to an ECM-presented ligand *via* multiphoton patterning (Figure 4f-i, Supplementary Figure 10 and Supplementary Movies 1-2). Collectively, this data demonstrates dynamic control over multiple factors in time and space with unmatched precision, as well as the first 4D regulation of site-specifically modified proteins within materials.

Encouraged that mCherry, mCerulean, and EGFP each retained their fluorescence and spatial patterning for several weeks following hydrogel tethering, we sought to determine whether we could confine enzymatic activity to user-specified gel subvolumes. Utilizing bla-*o*NB-N_3, we functionalized and patterned gels through mask-based protein photoremoval. Protein-patterned gels were treated with 7-thiophenylacetamido-3-thioacetoxymethyl-3-cephem-4-carboxylate[42] (thioacetate cefalotin, Supplementary Methods), a thiocephalosporin that eliminates a proton and a thiolate ion following β-lactam enzymatic hydrolysis that reduce a water-soluble yellow phenazine into a green water-insoluble precipitate (Figure 5a-b). Phase contrast microscopy indicated changes in localized refractive index, corresponding to enzyme-induced precipitation confined to bla-modified regions within the gel (Figure 5c, Supplementary Figure 11). We believe this to be the first successful example of confining enzymatic activity to photopatterned locations within a material, a task enabled by site-specific modification and that is likely to prove useful in enzymatically regulating critical ECM parameters.

Having demonstrated that sortagged enzymes remain active when photopatterned within gels and that gel formation and modification chemistries were cytocompatible (Supplementary Figure 12), we tested the ability of these techniques to direct local cell function using immobilized growth factors. HeLa cells transfected with the EKAREV FRET reporter for MAPK activation[38] were encapsulated in materials uniformly functionalized with EGF-*o*NB-N_3. Following complete bulk protein photorelease, cells displayed basal levels of MAPK activation; those where EGF remained immobilized elicited significantly higher (~2 fold) intracellular signaling (Figure 6d-e). The extent of FRET responses for cells in 3D was consistent with 2D studies involving soluble EGF (Supplementary Figures 13 and Supplementary Movie 3) and is not directly affected by light treatments used for gel photomodulation (Supplementary Figure 14). Taking advantage of the spatial control afforded by protein photorelease, gels with patterned EGF were created through masked exposure; MAPK activation remained high in gel subvolumes still functionalized with EGF, but returned to basal levels in those where the protein had been photoreleased. Since MAPK signaling plays a key role in regulating cell proliferation, migration, and differentiation, its patterned activation represents a powerful step towards regulating advanced cell fates with spatiotemporal control. We believe that these results are the first example of photopatterned regulation over a specific biochemical pathway in a 3D material.

An added benefit of using STEPL to modify proteins for material decoration is its compatibility with many standard protein engineering strategies. Though the photoremovable EGF proved successful in spatially regulating MAPK activation in 3D gels, its location cannot be directly visualized during experimentation. To address this limitation, we constructed an expression vector for an EGFP-EGF fusion and performed STEPL using H-GGGGDDK(*o*NB-N_3)-NH_2 to

generate EGFP-EGF-*o*NB-N_3 (Supplementary Methods, Supplementary Figure 15). Taking advantage of its fluorescence, bioactivity, tetherability, and photoreleasability, we first used this tetrafunctional protein to pattern proliferation through dynamic EGF stimulation (Figure 6ab). Epidermal A431 cells were seeded on hydrogels containing interspaced lines of EGFP-EGF-*o*NB-N_3. The immobilized EGFP-EGF remained effective in driving proliferation, where cell patterning was visibly evident by Day 3 (Supplementary Figure 16); functionalized regions yielded ~2-fold increased cell densities relative to those lacking EGF by Day 6. Control experiments with patterned EGFP exhibited homogenous surface coverage with no significant difference in cell localization based on the underlying fluorescent protein pattern at any observed time point (Supplementary Figure 17). To assay the effects of dynamically patterned EGF stimulation on cell function, a parallel experiment was constructed in which the EGFP-EGF was photoreleased from one half of each individual line-patterned gel three days into culture. Though the persistently functionalized gel portions exhibited the expected patterning in cell density, uniform surface coverage was observed across the photoreleased gel portions where presumably cells had redistributed through migration to eliminate any previously patterned heterogeneity (Supplementary Figure 18). 3D experiments involving encapsulated HeLa cells yielded similar results, where spheroid growth was enhanced with persistently patterned EGFP-EGF (Supplementary Figures 19-21). Through reversibly controlled presentation of bioactive growth factors, we demonstrate newfound ability to modulate local proliferation/migration of cells in 2D and 3D.

Armed with the EGFP-EGF-*o*NB-N_3 tetrafunctional chimera, we sought to demonstrate that photoreleased proteins could influence dynamic biological fate with resolutions previously

inaccessible to biomaterials-based approaches. EGF binds cell surface protein epidermal growth factor receptor (EGFR), yielding an activated transmembrane protein that undergoes homodimerization. Canonical EGFR activation is coupled with membrane endocytosis, receptor trafficking, and downstream signal transduction. Though matrix-bound EGF binds EGFR, growth factor tethering inhibits ligand-receptor internalization, endocytotic trafficking, and canonical signaling[43,44]. We hypothesized that photoliberation of soluble EGFR-EGF could be used to "turn on" canonical EGFR activation locally within culture, and that downstream endosome formation could be visualized with fluorescent microscopy (Figure 6c, Supplementary Figure 22). To test this hypothesis, A431 cells were encapsulated in gels modified with EGFP-EGF-*o*NB-N_3. Confocal imaging revealed a fluorescent halo initially outlining each cell, indicating ligand-receptor binding and the presence of concentrated membrane-bound EGFP-EGF (Figure 6d). Multiphoton laser scanning lithography was used to selectively release the EGFP-EGF protein on one side of an individual encapsulated cell, triggering EGFP-EGF untethering and local endocytic vesicle formation, visible in <5 minutes and concentrated in the regions of light exposure (Figure 6ef). Cells within the same imaging window (~50 μm away) were unaffected by the photoreleased EGF, further indicating that activation could be specified with single micron-scale precision. Control studies involving photoreleasable EGFP did not yield endocytosis (Supplementary Figure 23). We believe this to be the first demonstration of using dynamic materials to govern 3D fate with single cell and/or subcellular resolution.

The results described here introduce and highlight the sortase-mediated transpeptidation as a uniquely powerful strategy to create a diverse library of homogenous, singly modified proteins with non-natural functionality. Sortagged proteins can be efficiently expressed and purified by

STEPL, and exhibit near-native bioactivity while affording the ability to decorate biomaterials in a user-dictated manner. By specifying reactive handle identity, functional proteins can be reversibly immobilized within hydrogels with excellent spatiotemporal resolution through a variety of bioorthogonal photochemical reactions. Such patterned control over niche biochemical properties with homogenous proteins permits unprecedented regulation of complex biological functions and cellular pathways. We expect that this approach will prove useful in probing the effects of ECM-presented cues on single cell fate and in the design of materials for tissue engineering, potentially opening the door to multi-lineage patterning of 3D stem cell differentiation.

References:

1. Lutolf, M. P., Gilbert, P. M. & Blau, H. M. Designing materials to direct stem-cell fate. *Nature* **462,** 433–441 (2009).
2. Tibbitt, M. W. & Anseth, K. S. Dynamic Microenvironments: The Fourth Dimension. *Sci. Transl. Med.* **4,** (2012).
3. Baker, B. M. & Chen, C. S. Deconstructing the third dimension – how 3D culture microenvironments alter cellular cues. *J. Cell Sci.* **125,** (2012).
4. DeForest, C. A. & Anseth, K. S. Advances in Bioactive Hydrogels to Probe and Direct Cell Fate. *Annu. Rev. Chem. Biomol. Eng.* **3,** 421–444 (2012).
5. Burdick, J. A. & Murphy, W. L. Moving from static to dynamic complexity in hydrogel design. *Nat. Commun.* **3,** 1269 (2012).
6. Langer, R. & Vacanti, J. P. Tissue Engineering. *Science* **260,** 920–926 (1993).
7. Lee, K. Y. & Mooney, D. J. Hydrogels for tissue engineering. *Chem. Rev.* **101,** 1869–1879 (2001).
8. Langer, R. & Tirrell, D. A. Designing materials for biology and medicine. *Nature* **428,** 487–492 (2004).
9. Cushing, M. C. & Anseth, K. S. Hydrogel cell cultures. *Science* **316,** 1133–1134 (2007).
10. Tibbitt, M. W. & Anseth, K. S. Hydrogels as Extracellular Matrix Mimics for 3D Cell Culture. *Biotechnol. Bioeng.* **103,** 655–663 (2009).
11. Seliktar, D. Designing Cell-Compatible Hydrogels for Biomedical Applications. *Science* **336,** 1124–1128 (2012).
12. Lutolf, M. P. & Hubbell, J. A. Synthetic biomaterials as instructive extracellular microenvironments for morphogenesis in tissue engineering. *Nat. Biotechnol.* **23,** 47–55

(2005).

13. Zhang, Y. S. & Khademhosseini, A. Advances in engineering hydrogels. *Science* **356,** (2017).

14. Tam, R. Y., Smith, L. J. & Shoichet, M. S. Engineering Cellular Microenvironments with Photo- and Enzymatically Responsive Hydrogels: Toward Biomimetic 3D Cell Culture Models. *Acc. Chem. Res.* **50,** 703–713 (2017).

15. Caliari, S. R. & Burdick, J. A. A practical guide to hydrogels for cell culture. *Nat. Methods* **13,** 405–414 (2016).

16. Rosales, A. M. & Anseth, K. S. The design of reversible hydrogels to capture extracellular matrix dynamics. *Nat. Rev. Mater.* **1,** 15012 (2016).

17. Ruskowitz, E. R. & DeForest, C. A. Photoresponsive biomaterials for targeted drug delivery and 4D cell culture. *Nat. Rev. Mater.* **3,** 17087 (2018).

18. Luo, Y. & Shoichet, M. S. A photolabile hydrogel for guided three-dimensional cell growth and migration. *Nat. Mater.* **3,** 249–253 (2004).

19. Hahn, M. S., Miller, J. S. & West, J. L. Three-dimensional biochemical and biomechanical patterning of hydrogels for guiding cell behavior. *Adv. Mater.* **18,** 2679–2684 (2006).

20. DeForest, C. A., Polizzotti, B. D. & Anseth, K. S. Sequential click reactions for synthesizing and patterning three-dimensional cell microenvironments. *Nat. Mater.* **8,** 659–664 (2009).

21. DeForest, C. A., Sims, E. A. & Anseth, K. S. Peptide-functionalized click hydrogels with independently tunable mechanics and chemical functionality for 3D cell culture. *Chem. Mater.* **22,** 4783–4790 (2010).

22. DeForest, C. A. & Anseth, K. S. Cytocompatible click-based hydrogels with dynamically tunable properties through orthogonal photoconjugation and photocleavage reactions. *Nat. Chem.* **3,** 925–931 (2011).

23. DeForest, C. A. & Anseth, K. S. Photoreversible patterning of biomolecules within click-based hydrogels. *Angew. Chemie - Int. Ed.* **51,** 1816–1819 (2012).

24. Wylie, R. G., Ahsan, S., Aizawa, Y., Maxwell, K. L., Morshead, C. M. & Shoichet, M. S. Spatially controlled simultaneous patterning of multiple growth factors in three-dimensional hydrogels. *Nat. Mater.* **10,** 799–806 (2011).

25. Mosiewicz, K. A., Kolb, L., van der Vlies, A. J., Martino, M. M., Lienemann, P. S., Hubbell, J. A., Ehrbar, M., Lutolf, M. P., Vlies, A. J. van der, Martino, M. M., Lienemann, P. S., Hubbell, J. A., Ehrbar, M. & Lutolf, M. P. In situ cell manipulation through enzymatic hydrogel photopatterning. *Nat. Mater.* **12,** 1071–1077 (2013).

26. Griffin, D. R., Borrajo, J., Soon, A., Acosta-Velez, G. F., Oshita, V., Darling, N., Mack, J., Barker, T., Iruela-Arispe, M. L. & Segura, T. Hybrid Photopatterned Enzymatic Reaction (HyPER) for in Situ Cell Manipulation. *Chembiochem* **15,** 233–242 (2014).

27. DeForest, C. A. & Tirrell, D. A. A photoreversible protein-patterning approach for guiding stem cell fate in three-dimensional gels. *Nat. Mater.* **14,** 523–531 (2015).

28. Fisher, S. A., Baker, A. E. G. & Shoichet, M. S. Designing Peptide and Protein Modified Hydrogels: Selecting the Optimal Conjugation Strategy. *J. Am. Chem. Soc.* **139,** 7416–7427 (2017).

29. Baslé, E., Joubert, N. & Pucheault, M. Protein Chemical Modification on Endogenous Amino Acids. *Chem. Biol.* **17,** 213–227 (2010).

30. Rabuka, D. Chemoenzymatic methods for site-specific protein modification. *Curr. Opin.*

Chem. Biol. **14,** 790–796 (2010).

31. Rabuka, D., Rush, J. S., deHart, G. W., Wu, P. & Bertozzi, C. R. Site-specific chemical protein conjugation using genetically encoded aldehyde tags. *Nat. Protoc.* **7,** 1052–1067 (2012).

32. Kulkarni, C., Kinzer-Ursem, T. L. & Tirrell, D. A. Selective Functionalization of the Protein N Terminus with N-Myristoyl Transferase for Bioconjugation in Cell Lysate. *ChemBioChem* **14,** 1958–1962 (2013).

33. Chen, I., Howarth, M., Lin, W. & Ting, A. Y. Site-specific labeling of cell surface proteins with biophysical probes using biotin ligase. *Nat. Methods* **2,** 99–104 (2005).

34. Guimaraes, C. P., Witte, M. D., Theile, C. S., Bozkurt, G., Kundrat, L., Blom, A. E. M. & Ploegh, H. L. Site-specific C-terminal and internal loop labeling of proteins using sortase-mediated reactions. *Nat. Protoc.* **8,** 1787–1799 (2013).

35. Mao, H., Hart, S. A., Schink, A. & Pollok, B. A. Sortase-mediated protein ligation: a new method for protein engineering. *J. Am. Chem. Soc.* **126,** 2670–1 (2004).

36. Mazmanian, S. K., Liu, G., Hung, T. T. & Schneewind, O. Staphylococcus aureus sortase, an enzyme that anchors surface proteins to the cell wall. *Science* **285,** 760–763 (1999).

37. Warden-Rothman, R., Caturegli, I., Popik, V. & Tsourkas, A. Sortase-tag expressed protein ligation: Combining protein purification and site-specific bioconjugation into a single step. *Anal. Chem.* **85,** 11090–11097 (2013).

38. Komatsu, N., Aoki, K., Yamada, M., Yukinaga, H., Fujita, Y., Kamioka, Y. & Matsuda, M. Development of an optimized backbone of FRET biosensors for kinases and GTPases. *Mol. Biol. Cell* **22,** 4647–56 (2011).

39. Hermanson, G. T. *Bioconjugate Techniques*. (Academic Press, 2013).

40. Farahani, P. E., Adelmund, S. M., Shadish, J. A. & DeForest, C. A. Photomediated Oxime Ligation as a Bioorthogonal Tool for Spatiotemporally-Controlled Hydrogel Formation and Modification. *J. Mater. Chem. B* **5,** 4435–4442 (2017).

41. Kloxin, A. M., Kasko, A. M., Salinas, C. N. & Anseth, K. S. Photodegradable Hydrogels for Dynamic Tuning of Physical and Chemical Properties. *Science* **324,** 59–63 (2009).

42. Bieniarz, C., Young, D. F. & Cornwell, M. J. Chromogenic redox assay for beta-lactamases yielding water-insoluble products. I. Kinetic behavior and redox chemistry. *Anal. Biochem.* **207,** 321–8 (1992).

43. Kuhl, P. R. & Griffith-Cima, L. G. Tethered epidermal growth factor as a paradigm for growth factor–induced stimulation from the solid phase. *Nat. Med.* **2,** 1022–1027 (1996).

44. Fan, V. H., Au, A., Tamama, K., Littrell, R., Richardson, L. B., Wright, J. W., Wells, A. & Griffith, L. G. Tethered Epidermal Growth Factor Provides a Survival Advantage to Mesenchymal Stem Cells. *Stem Cells* **25,** 1241–1251 (2007).

Acknowledgements:

The authors recognize and thank Drs. R. Seifert and D. Hailey of the University of Washington Garvey Imaging Center for their ongoing support and advice, Drs. F. Watt and T. Hiratsuka (King's College London) for helpful discussion on visualizing MAPK activation, Dr. M. Matsuda (Kyoto University) for gifting the HeLa cells transfected with EKAREV FRET sensor, as well as Drs. R. Warden-Rothman and A. Tsourkis (University of Pennsylvania) for providing the pSTEPL plasmid[37]. The authors thank B. Badeau for assistance in synthesizing N_3-*o*NB-OSu, S. Adelmund for providing BCN-OSu, and A. Im for help with protein purification optimization. We gratefully acknowledge support from S. Edgar at the UW Mass Spectrometry Center as well as that from the NIH and N. Peters at the UW W. M. Keck Microscopy Center (S10 OD016240). This work was supported by a University of Washington Faculty Startup Grant (C.A.D.), a Jaconette L. Tietze Young Scientist Research Award (C.A.D.), and a CAREER Award (DMR 1652141, C.A.D.) from the National Science Foundation.

Author contributions:

For this manuscript, J.A.S. and C.A.D. conceived and designed the experiments; J.A.S. and G.M.B. performed the experiments; J.A.S. and C.A.D. analyzed the data and prepared the figures; J.A.S. and C.A.D. wrote the paper.

Competing financial interests:

The authors declare no competing financial interests.

Material and Data Availability:

Plasmids and data that support the findings of this study are available from the corresponding author upon reasonable request.

Methods:

Synthesis of polyglycine probes for sortagging. Polyglycine-containing peptides [H-GGGGDDK(N_3)-NH_2, H-GGGGDDK(CHO)-NH_2, H-GGGGDDK(*o*NB-N_3)-NH_2, H-GGGG-*o*NB-DDK(CHO)-NH_2] were synthesized through standard Fmoc solid-phase methodologies involving a butyloxycarbonyl-protected N-terminal glycine and a 4-methyltrity (Mtt)-protected C-terminal lysine reside. Following selective deprotection of Mtt (1% trifluoroacetic acid, TFA, in dichloromethane, DCM) on resin, azide (N_3), aldehyde (CHO), and photoreleasable azide (*o*NB-N_3) functionality were installed respectively by condensation with 4-azidobutanoic acid, 4-formylbenzoic acid, or 4-(4-(1-(4-azidobutanoyloxy)ethyl)-2-methoxy-5-nitrophenoxy)butanoic acid and the ε-amino group of the C-terminal lysine. Resin was washed (dimethylformamide, DMF, 3x; DCM, 3x) prior to peptide cleavage/deprotection (95:5 TFA:H_2O, 20 mL, 2 hr) and precipitation (diethyl ether, 180 mL, 0 °C, 2x). The crude peptide was purified *via* semi-preparative reversed-phase high-performance liquid chromatography using a 55-minute gradient (5–100% of acetonitrile and 0.1% TFA in H_2O) and lyophilized to give final product. Peptide purity was confirmed by matrix-assisted laser desorption/ionization time-of-flight mass spectrometry. Complete synthetic details and characterization are given in Supplementary Methods.

Generation of homogenous protein-peptide conjugates by STEPL. STEPL plasmids for EGFP, mCherry, mCerulean, bla, EGF, FGF, and EGFP-EGF were constructed from pSTEPL[37] using standard cloning techniques (Supplementary Methods) and transformed into BL21(DE3) *E. coli* (Thermo Fisher). For protein expression, transformants were grown at 37 °C in lysogeny

broth containing ampicillin (100 μg mL^{-1}) until an optical density of 0.6 (λ = 600 nm). Expression was induced with isopropyl β-D-1-thiogalactopyranoside (0.5 mM) and then agitated overnight at 18 °C. Cells were harvested *via* centrifugation and lysed by sonication. Clarified lysate was loaded onto HisPur Ni-NTA resin (ThermoFisher), which was washed (20 mM Tris, 50 mM NaCl, 20 mM imidazole) to remove unbound proteins. Following treatment of the resin with polyglycine probe of interest (20x, 4 h, 37 °C), sortagged proteins were eluted and purified by dialysis (molecular weight cut-off, MWCO ~10 kDa). Protein identity and purity was confirmed by liquid chromatography-tandem mass spectrometry, sodium dodecyl sulfate polyacrylamide gel electrophoresis, and gel shift analysis. Protein concentrations were determined by ultraviolet absorption (λ = 280 nm) and bicinchoninic acid assay prior to use. Complete experimental details are given in Supplementary Methods.

Random modification of proteins by NHS chemistry. Statistically modified proteins were prepared by reacting N_3-OSu (0x, 0 μM; 10x, 300 μM; 100x, 3 mM; 1000x, 30 mM) with protein (30 μM) in phosphate buffered saline (PBS, 900 μL) and DMF (100 μL) overnight at room temperature. Resulting protein solutions were purified with Zeba™ Spin Desalting Columns (MWCO ~ 7 kDa, Thermo Fisher) and buffer-exchanged into fresh PBS. Protein concentrations were determined by ultraviolet absorption (λ = 280 nm) and bicinchoninic acid assay prior to use.

Activity determination of native and modified proteins. EGFP, mCherry, and mCerulean fluorescence was quantified on a fluorescent plate reader (EGFP: $\lambda_{excitation}$ = 470 nm, $\lambda_{emission}$ = 530 nm; mCherry: $\lambda_{excitation}$ = 575 nm, $\lambda_{emission}$ = 620 nm; mCerulean: $\lambda_{excitation}$ = 430 nm, $\lambda_{emission}$

= 475 nm). Bla enzymatic activity was measured through a chromogenic assay, whereby bla (1 ng) was incubated with nitrocefin (2 mM) in PBS (100 μL). Sample absorbance (λ_{abs} = 386 nm) was measured over time at 37 °C; the initial slope was calculated as a measure of the k_{cat} of the enzyme. To determine EGF activity, HeLa cells expressing EKAREV[38] were plated in a 96-well plate (5,000 cells well^{-1}) and allowed to attach overnight in Dulbecco's Modified Eagle Medium (DMEM) (Life Technologies) supplemented with fetal bovine serum (FBS, 10%). 16 hours prior to imaging, cells were transitioned to serum-free DMEM. Time-series images (20 sec interval) were acquired on a fluorescent confocal microscope ($\lambda_{excitation}$ = 405 nm, 1% argon laser power; $\lambda_{emission,CFP}$ = 450-484 nm, $\lambda_{emission,YFP}$ = 520-524 nm) following stimulation with EGF (12.5 nM) in serum-free DMEM. The YFP/CFP FRET response ratio was calculated for each frame (ImageJ) and plotted over time. The relative activity of each EGF species was taken as the initial rate of change of the FRET response after EGF stimulation, normalized to native EGF. Alternatively, EGF activity was determined through a commercially available DNA synthesis assay (Click-iT EdU Alexa Fluor 488, Thermo Fisher). NIH3T3 cells were placed in a 96-well plate (5,000 cells well^{-1}) and cultured overnight in DMEM containing FBS (10%). Cells were washed with PBS (2x) and transferred to serum-free DMEM. After one day, cells were transitioned to serum-free DMEM containing 5-Ethynyl-2'-deoxyuridine (10 μM) with or without EGF (100 ng mL^{-1}). After two days of culture, cells were fixed in formaldehyde and processed following kit manufacturer recommendations. The relative activity of each EGF species was taken as the percentage of cells actively synthesizing DNA after EGF stimulation, normalized to unmodified EGF. FGF activity was determined through a proliferation assay using a commercially available assay (Quant-iT PicoGreen, Thermo Fisher) for dsDNA content. NIH3T3 cells (5,000 cells well^{-1}) were cultured overnight in 96-well plate in DMEM containing

FBS (10%) prior to being transferred to serum-free DMEM. After one day, cells were transferred to serum-free DMEM with or without FGF (100 ng mL^{-1}), incubated for two days, and assayed following manufacturer protocol. The relative activity of each FGF species corresponds to the total dsDNA content, normalized to unmodified FGF.

Formation of SPAAC-based hydrogels. A solution of PEG-tetraBCN (M_n ~ 20,000 Da, 4 mM), N_3-PEG-N_3 (M_n ~ 3,500 Da, 8 mM, Supplementary Methods), and N_3-TEG-ONH-NPPOC (0.1 mM) was prepared in PBS. Network formation was allowed to proceed for 1 hour between Rain-X®-treated glass slides with silicone rubber spacers (McMaster-Carr, 0.5 mm thick). The slides were separated, and gels were equilibrated overnight in PBS prior to use.

Photopatterning conditions for protein tethering and release. For photolithographic patterning, hydrogels were exposed to collimated UV light (λ = 365 nm, 10 mW cm^{-2}, 0 – 1200 s) through a patterned chrome photomask (Photo Sciences) using a Lumen Dynamics OmniCure S1500 Spot UV Curing system equipped with an internal 365 nm band-pass filter and a second in-line 360 nm cut-on longpass filter. Protein gradients were created by moving an opaque plate attached to a programmable linear motion stage over gels during light exposure at various rates (0.3 – 2.4 mm min^{-1}). For 3D patterning experiments within gels, an Olympus FV1000 MPE BX61 Multi-photon Microscope with a 20x objective was used. ROIs were scanned 16 times with pulsed laser light (λ = 740 nm, 50% laser power) with a 2.5 μm z-interval to generate 3D patterns. After NPPOC cleavage, gels were incubated for 8 hours with aldehyde-tagged protein (100 μM in PBS) at room temperature and protected from light. To remove unbound protein, gels were gently agitated in PBS (16 h) prior to imaging. Following light exposure, gels

containing photoreleasable proteins were incubated in PBS (16 h) prior to analysis. This process was repeated iteratively for patterning of multiple proteins. Experiments involving patterning of fluorescent proteins were visualized by fluorescent confocal or multiphoton microscopy, while those involving immobilized bla were imaged by phase-contrast microscopy. For experiments involving encapsulated mammalian cells, PBS was replaced with culture media during gel formation and patterning.

Spatial assessment of bla enzymatic activity. SPAAC-based gels uniformly functionalized with bla-*o*NB-N_3 (30 μM) were subjected to masked light (λ = 365 nm, 10 mW cm^{-2}, 10 min). Protein-patterned gels were incubated with thioacetate cefalotin (5 mM, Supplementary Methods) and phenazine methosulfate (6.5 mM) in PBS (37 °C, 1 h). The gels were then washed with PBS (3x, 15 min) prior to visualization by phase contrast microscopy.

Encapsulation of MAPK FRET reporter cells. HeLa cells stably transfected with the EKAREV FRET sensor[38] were expanded in high-glucose DMEM supplemented with FBS (10%) and penicillin/streptomycin (1%) in a 5% CO_2 atmosphere at 37 °C. Culture medium was changed every two to three days, and cells were passaged at ~70% confluency. HeLa cells were encapsulated (2 x 10^6 cells mL^{-1}) in SPAAC-based gels (10 μL) modified with EGF-*o*NB-N_3 (12.5 nM) and an N_3-GRGDS-NH_2 peptide (Supplementary Methods, 100 μM) for cell attachment. Photopatterning was performed 24 hours after encapsulation. Prior to FRET imaging (16 h), culture media was replaced with serum-free DMEM containing penicillin/streptomycin (1%).

Visualization of patterned MAPK signaling. HeLa EKAREV-laden hydrogels were imaged using a Leica SP8X confocal microscope at a constant distance below gel surface (100 μm). EKAREV was excited using an argon laser (λ = 405 nm, 10% laser power); CFP excitation was monitored from $\lambda_{emission,CFP}$ = 450-484 nm, while YFP fluorescence was measured from $\lambda_{emission,YFP}$ = 520-524 nm. After image acquisition, background fluorescence was subtracted, and the YFP/CFP ratio for each pixel of the image was calculated using ImageJ. FRET response ratios were visualized as a blue-green-red color map.

Cell response to dynamically patterned EGFP-EGF. EGFP-EGF-*o*NB-N_3 (25 μM) was conjugated (25 °C, 1 hr) to PEG-tetraBCN (M_n ~ 20,000 Da, 4 mM). EGFP-EGF-modified hydrogels (5 μL) were formed (1 hr) between Rain-X®-treated glass slides with silicone rubber spacers (McMaster-Carr, 0.5 mm thick) with cell-adhesive and matrix metalloproteinase-degradable crosslinker N_3-GGRGDSPGGPQGIWGQGK(N_3)-NH_2 (Supplementary Methods, 8 mM). After removal from glass slide chamber, gels were exposed to masked collimated UV light (λ = 365 nm, 10 min, 10 mW cm^{-2}) through a slitted photomask containing 400 μm wide line features and soaked in PBS overnight. Gels were swollen (1 hr) in DMEM containing FBS (10%) prior to cell seeding. A431 cells (1 x 10^7 cells mL^{-1}) were added to the top of gels as a droplet (10 μL) and allowed to attach (1 hr, 37 °C) prior to media addition. Gels were swollen in DMEM containing FBS (10%) and penicillin/streptomycin (1%) overnight prior to imaging (condition ①). Gel media was supplemented with bovine serum albumin (BSA, 0.1%) and cells maintained in culture (37 °C, 5% CO_2). Three days after cell seeding, a portion of the hydrogels were exposed to a second round of photopatterning; one half of each treated gel was exposed to UV light (λ = 365 nm, 10 min, 10 mW cm^{-2}) while the other half was left unexposed. In all cases,

gels were maintained in DMEM containing FBS (10%), penicillin/streptomycin (1%), and BSA (0.1%) for an additional three days prior to analysis (conditions ② and ③). At the end of each treatment condition, cells were fixed in paraformaldehyde (1%, 30 min), stained with DAPI (0.15 μg/mL, 30 min), and visualized *via* fluorescence microscopy. Image analysis was performed for each condition using ImageJ, quantifying the normalized intensity profile for EGFP, nuclei, and optical transmission across the gel perpendicular to photopatterned lines. Whole-gel images were performed on an Epson Perfection 4490 Photo document scanner.

Encapsulated cell response to subcellular photoreleased EGFP-EGF. A431 cells (2 x 10^6 cells mL^{-1}) were encapsulated in SPAAC hydrogels (5 μL) containing EGFP-EGF-*o*NB-N_3 (125 nM) and N_3-GRGDS-NH_2 peptide (Supplementary Methods, 1 mM) affixed to an azide-functionalized slide (Supplementary Methods). The cells were cultured for 48 hr in DMEM supplemented with FBS (10%) and penicillin/streptomycin (1%) before transferring to phenol red-free DMEM containing FBS (10%) and penicillin/streptomycin (1%). Protein photorelease was performed *via* multiphoton laser scanning lithography (Olympus FV1000 MPE BX61 Multi-photon Microscope, 20x objective, 5x zoom, λ = 740 nm, 25% laser power, 16 scan repeats, z-interval = 2.5 μm), confined to a 40 μm x 30 μm x 5 μm subvolume bisecting an individual cell. ImageJ was used to calculate the difference in EGFP fluorescence pixel intensity accompanying photorelease.

Statistics:

Two-tailed t-tests assuming equal variance were performed to determine p values and statistical significance.

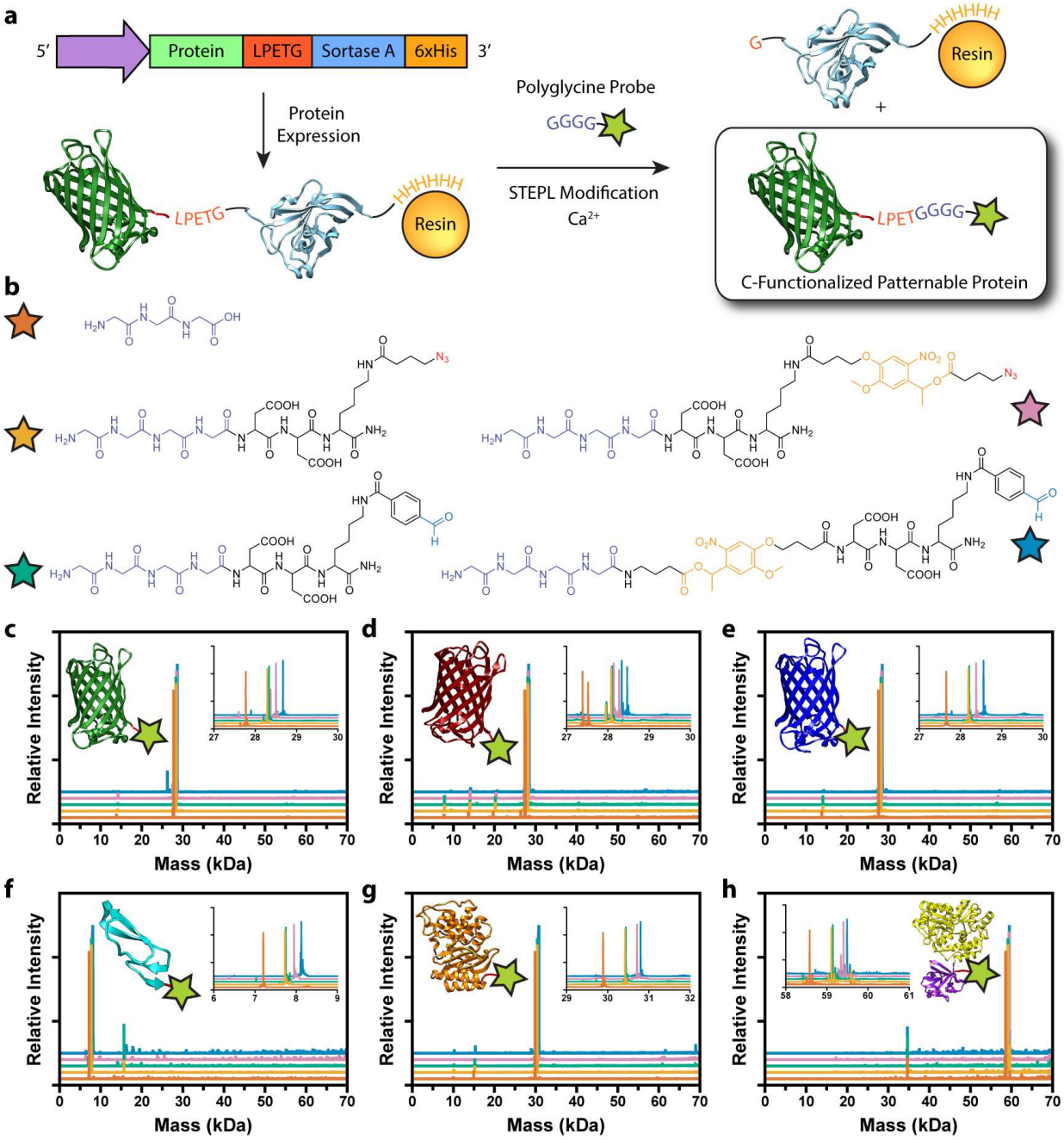

Figure 1 | Generation of sortagged protein library for biomaterial modification. a. Sortase-Tag Expressed Protein Ligation (STEPL) enables one-step protein biofunctionalization and purification of C-modified proteins for biomaterial decoration. Proteins appended with a genetically encoded sorting signal are expressed as a fusion with the sortase enzyme and a 6xHis tag. Following chromatographic isolation on Ni-NTA resin, intramolecular sortagging is

promoted by the addition of calcium and a polyglycine probe, catalyzing peptide ligation to the protein of interest and simultaneous displacement from the 6xHis-functionalized sortase A. Final protein functionality is defined by polyglycine compound identity. **b.** Five distinct polyglycine probes each with different reactive functional groups enabling biomaterial decoration were synthesized and exploited for STEPL: triglycine, H-GGGGDDK(N_3)-NH_2, H-GGGGDDK(CHO)-NH_2, H-GGGGDDK(*o*NB-N_3)-NH_2, H-GGGG-*o*NB-DDK(CHO)-NH_2 (denoted respectively with orange, tan, teal, pink, and blue stars). **c-h.** Whole-protein mass spectrometry of sortagged proteins (**c**, EGFP; **d**, mCherry; **e**, mCerulean; **f**, EGF; **g**, bla; **h**, FGF) indicates high sample purity and quantitative functionalization for all polyglycine probes. Curve color denotes probe identity following the same scheme as **b**. Double peaks in **d** indicate incomplete N-terminal methionine excision common to mCherry expression. Spectra in **c-h** correspond to observed masses from a single purification of each species.

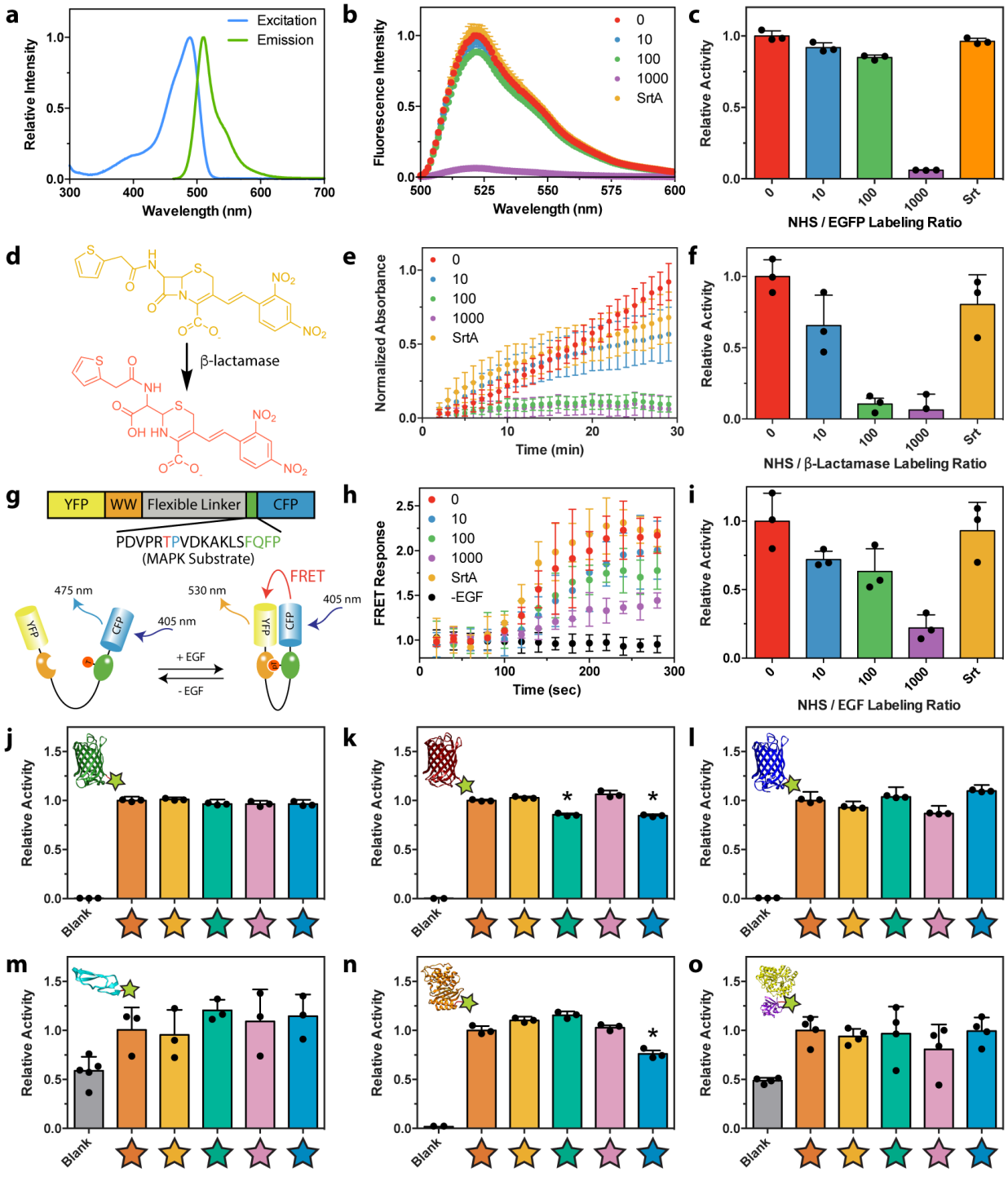

Figure 2 | Comparing activity of differently modified proteins. a-i. Bioactivity was compared for proteins azide-tagged by STEPL with H-GGGGDDK(N_3)-NH_2 or by conventional NHS labeling with varying molar excesses of N_3-OSu (0, 10, 100, 1000x). **a.** EGFP fluorescence was

used as a surrogate readout of its activity following protein modification. **b.** Fluorescence emission spectra was determined for modified EGFP ($\lambda_{excitation}$ = 470 nm). **c.** Increasing NHS modification led to a decrease in EGFP emission ($\lambda_{excitation}$ = 470 nm, $\lambda_{emission}$ = 530 nm), while sortagged EGFP retained native-like fluorescence. **d.** Bla activity was determined by its ability to degrade a chromogenic nitrocefin substrate, which changes from yellow to red upon β-lactam cleavage. **e.** Time-course spectrophotometric analyses (λ_{abs} = 386 nm) indicate nitrocefin degradation for NHS-modified and sortagged bla. **f.** Sortagged and unmodified bla exhibited statistically indistinguishable levels of bioactivity, as indicated by similar values for k_{cat}. Bla displayed high sensitivity to NHS labeling, likely due to the presence of a critical lysine residue in its active pocket. **g.** Activity of EGF was quantitatively determined with a HeLa cell line expressing EKAREV FRET reporter for MAPK activation. Functional EGF catalyzes phosphorylation of a MAPK substrate, resulting in an intramolecular association that colocalizes a Yellow Fluorescent Protein (YFP) and Cyan Fluorescent Protein (CFP) FRET pair. **h.** YFP/CFP FRET ratios following growth factor stimulation were determined for modified EGF. **i.** Increased NHS labeling of EGF yielded decreased bioactivity, as determined by the initial rate of change in FRET response, while the sortagged growth factor exhibited native levels of activity. **j-o.** Relative bioactivity of proteins (**j**, EGFP; **k**, mCherry; **l**, mCerulean; **m**, EGF; **n**, bla; **o**, FGF) sortagged with triglycine, H-GGGGDDK(N_3)-NH_2, H-GGGGDDK(CHO)-NH_2, H-GGGGDDK(*o*NB-N_3)-NH_2, and H-GGGG-*o*NB-DDK(CHO)-NH_2 (denoted respectively with orange, tan, teal, pink, and blue stars). * denotes conjugates with a statistically significant reduction in bioactivity ($p < 0.05$), as compared to the unmodified species (unpaired two-tailed t-test, $p = 1.3 \times 10^{-4}$ for mCherry-CHO, $p = 3.5 \times 10^{-4}$ for mCherry-*o*NB-CHO, $p = 3.2 \times 10^{-3}$ for bla-*o*NB-CHO). Error bars correspond to the standard deviation about the mean for biological

replicate experiments (n = 3 for studies involving fluorescent proteins, β-lactamase, and EGF; n = 4 for MBP-FGF).

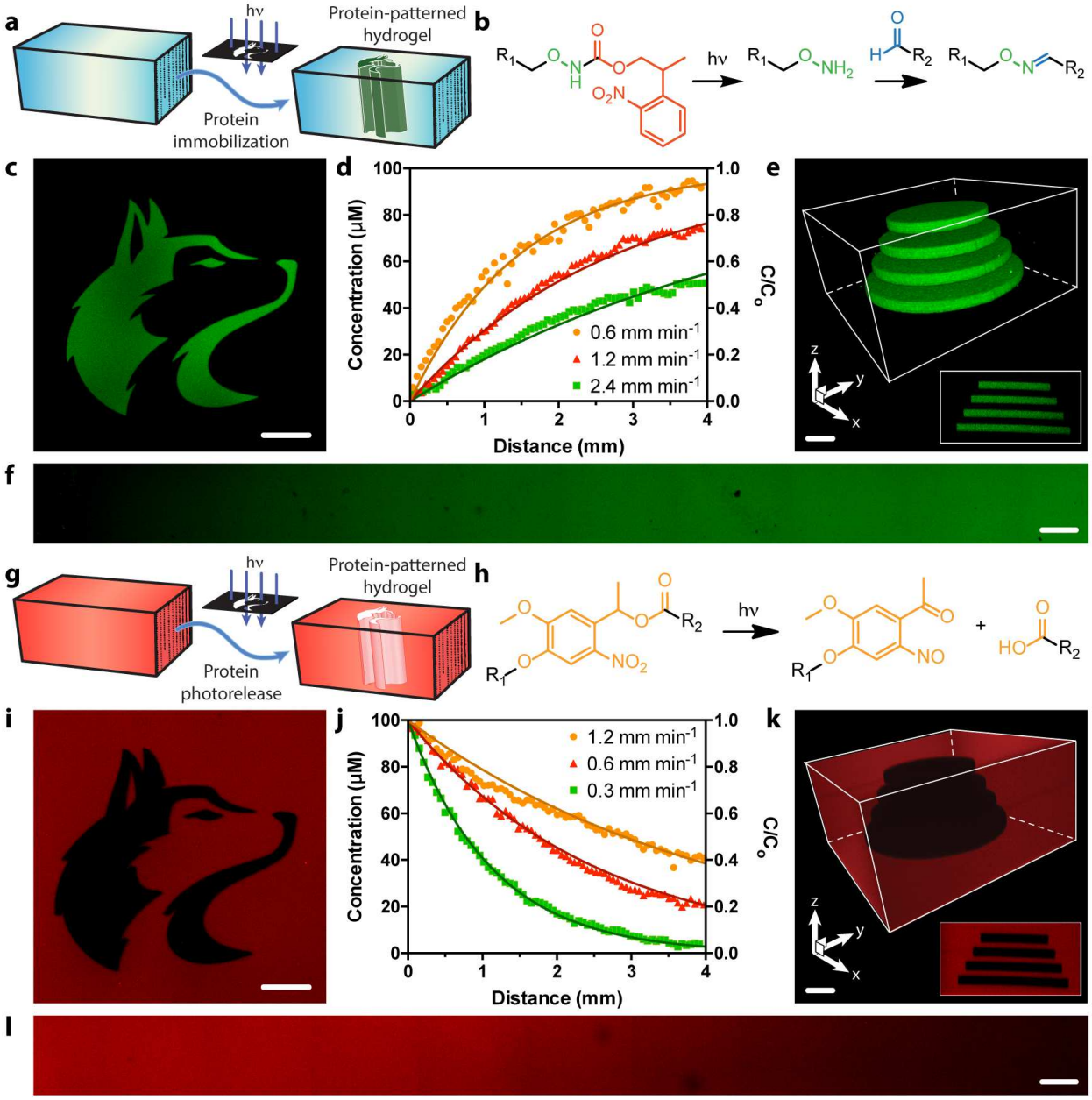

Figure 3 | Photopatterned alteration of hydrogel biomaterials with sortagged proteins. a-f. Photopatterned immobilization of sortagged proteins within gels. **a.** Proteins modified site-specifically with aromatic aldehydes are immobilized within SPAAC-based gels through photomediated oxime ligation. **b.** NPPOC-caged alkoxyamines distributed uniformly throughout gels (R_1) undergo irreversible β-elimination upon mild UV light exposure (λ = 365 nm or 740 nm). The deprotected alkoxyamines react with aldehyde-tagged proteins (R_2) to form stable

oxime linkages. **c.** Mask-based photolithography (λ = 365 nm) was used to immobilize discrete patterns of EGFP-CHO throughout the gel thickness. **d,f.** By exposing gel surfaces to linear gradients of light exposure (created by covering samples with an opaque photomask moving at rates of 0.6, 1.2, 2.4 mm min^{-1}, 10 mW cm^{-2}, λ = 365 nm), exponential protein gradients were generated in a dose-dependent manner. C_0 represents the highest possible protein concentration that can be immobilized (determined based on the 100 μM caged alkoxyamine included during gel formulation). **e.** Full 3D control over protein tethering within gels is achieved through multiphoton laser-scanning lithographic patterning (λ = 740 nm). **g-l.** Photopatterned release of sortagged proteins from gels. **g.** Site-specifically modified proteins are released from SPAAC-based gels through *ortho*-nitrobenzyl ester (*o*NB) photocleavage. **h.** *o*NB moieties linking the sortagged proteins (R_1) and the hydrogel (R_2) undergo rapid photoscission upon mild UV light exposure (λ = 365 nm or 740 nm). **i.** Mask-based photolithography (λ = 365 nm) was used to dictate discrete patterns of protein release from gels uniformly functionalized with mCherry-*o*NB-N_3. **j,l.** By exposing gel surfaces to linear gradients of light exposure (created by covering samples with an opaque photomask moving at rates of 0.3, 0.6, 1.2 mm min^{-1}, 10 mW cm^{-2}, λ = 365 nm), exponential protein gradients were generated in a dose-dependent manner. C_0 corresponds to the initial mCherry concentration included during gel formulation (100 μM). **k.** Full 3D control over protein release within gels is achieved through multiphoton laser-scanning lithographic patterning (λ = 740 nm). Immobilized protein concentrations in **d** and **j** are determined through fluorescence correlation. Solid curves in **d** and **j** are predicted by known NPPOC/*o*NB photocleavage kinetics. Images in **c**, **e**, **f**, **i**, **k**, and **l** correspond to representative individual gels imaged by fluorescence confocal microscopy. Data in **d** and **j** was derived from experiments involving single gels for each gradient light condition. Inset in **e** corresponds to a

maximum-intensity y-projection, while that in **k** corresponds to a minimum-intensity y-projection. Scale bars = 100 μm.

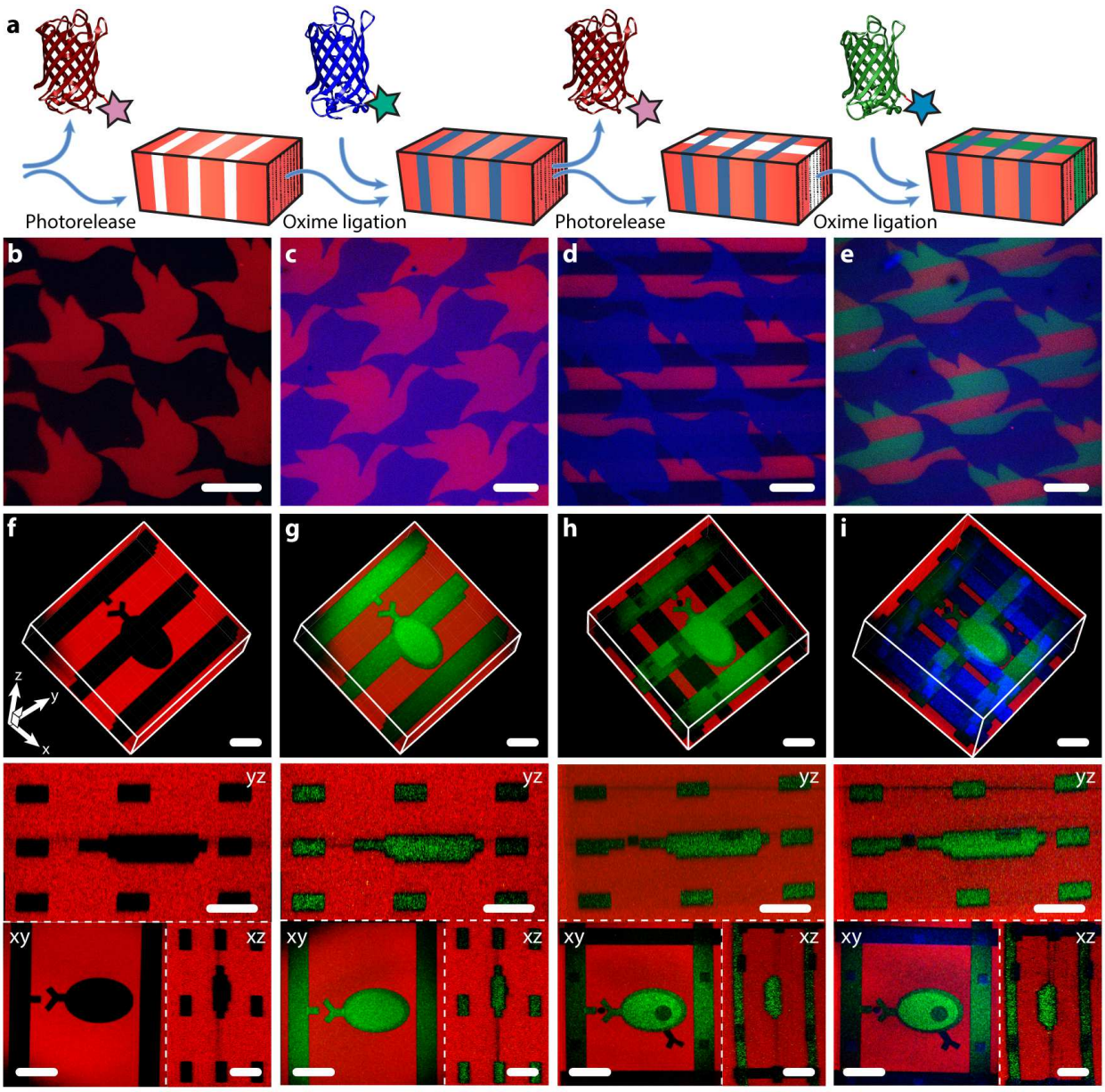

Figure 4 | 4D photoevolution of hydrogel biomaterials patterned with multiple sortagged proteins. a. Protein photorelease can be performed in concert with photomediated ligation of an aldehyde-tagged protein to create complex interconnected biochemical patterns. Iteration of this process enables 4D evolution of protein patterns within gels. **b-e.** Masked-based photolithographic techniques ($\lambda = 365$ nm) were utilized to control sequential protein patterning in defined shapes extending throughout the gel thickness. **b.** Following directed exposure of gels

uniformly functionalized with mCherry-*o*NB-N_3 (red), mCherry is released while uncaging sites for subsequent mCerulean-CHO (blue) immobilization by oxime ligation (**c**). **d.** A second round of directed light exposure released additional mCherry while leaving mCerulean patterns intact. **e.** EGFP-*o*NB-CHO (green) is immobilized in the uncaged alkoxyamine sites to create a trifunctional protein pattern. **f-i.** Evolution of trifunctional protein patterns was controlled in 3D space through multiphoton laser-scanning lithography (λ = 740 nm). Rows **f-i** correspond to 3D renderings of the photoevolved materials, where red channels represent minimum intensity projections and green and blue are maximum intensity projections, as well asxy, yz, and xz planar slices. **f**. Photorelease of mCherry-*o*NB-N_3 is followed by (**g**) protein backfilling with EGFP-*o*NB-CHO. **h**. Further treatment with pulsed laser light released both EGFP-*o*NB-CHO and mCherry-*o*NB-N_3 within user-specified gel sub-volumes while creating anchoring sites for (**i**) mCerulean-CHO immobilization. Images in **b**-**i** were generated using fluorescence confocal microscopy on a single gel throughout sequential patterning. Scale bars = 100 μm.

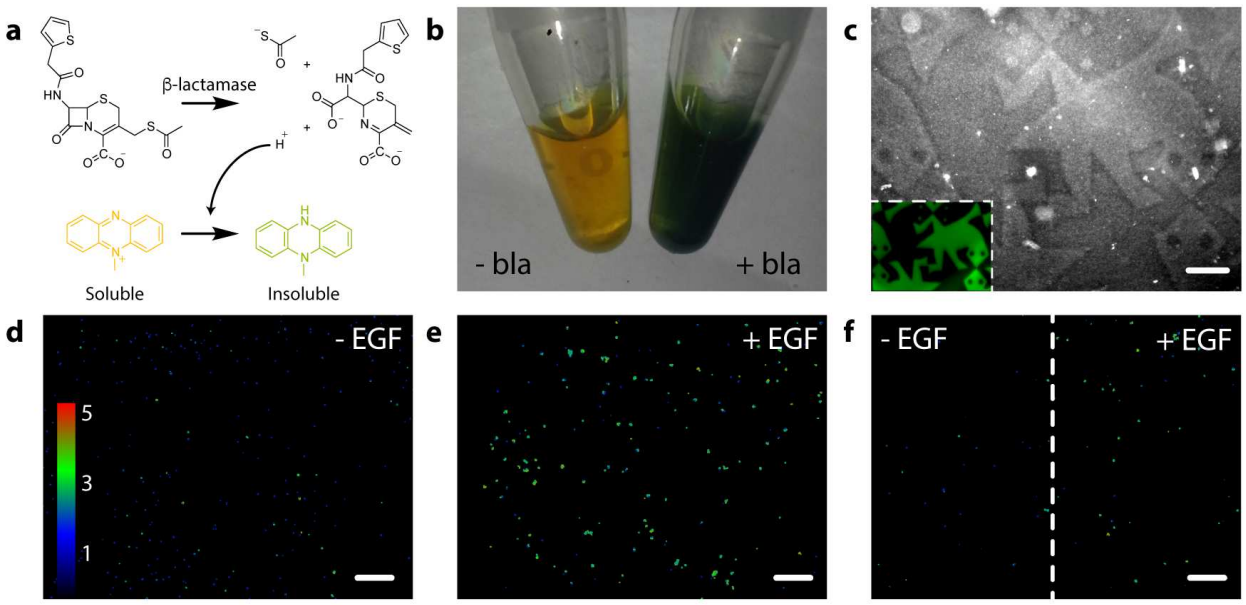

Figure 5 | Spatial patterning of gels with bioactive site-specifically modified enzymes and growth factors. a. Thioacetate cefalotin is hydrolyzed enzymatically by bla, eliminating proton and thiolate ions that reduce a water-soluble yellow phenazine into a green water-insoluble precipitate. **b.** In-solution treatment of thioacetate cefalotin (5 mM) and phenazine methosulfate (6.5 mM) with bla (30 μM) yields distinct color change and precipitate formation. **c.** Gels containing photopatterned regions of immobilized bla were visualized by phase contrast microscopy upon treatment with thioacetate cefalotin and phenazine methosulfate. Insoluble precipitation was confined to bla-modified gel subvolumes. Inset corresponds to an EGFP-modified gel with the same tessellated protein pattern. **d.** HeLa cells encapsulated in gels and expressing EKAREV FRET reporter for MAPK signaling exhibit basal signaling. **e.** Average intracellular MAPK activation increases ~2 fold when gels are uniformly functionalized with EGF (12.5 nM). **f.** High MAPK activation persisted in EGF-patterned gel regions, whereas no upregulation in MAPK levels is observed in unfunctionalized regions. Images in **d-f** represent color-coded FRET response normalized to basal MAPK activation, obtained from confocal z-

slices. All experiments were conducted in triplicate (n = 3) with similar results. Scale bars = 250 μm.

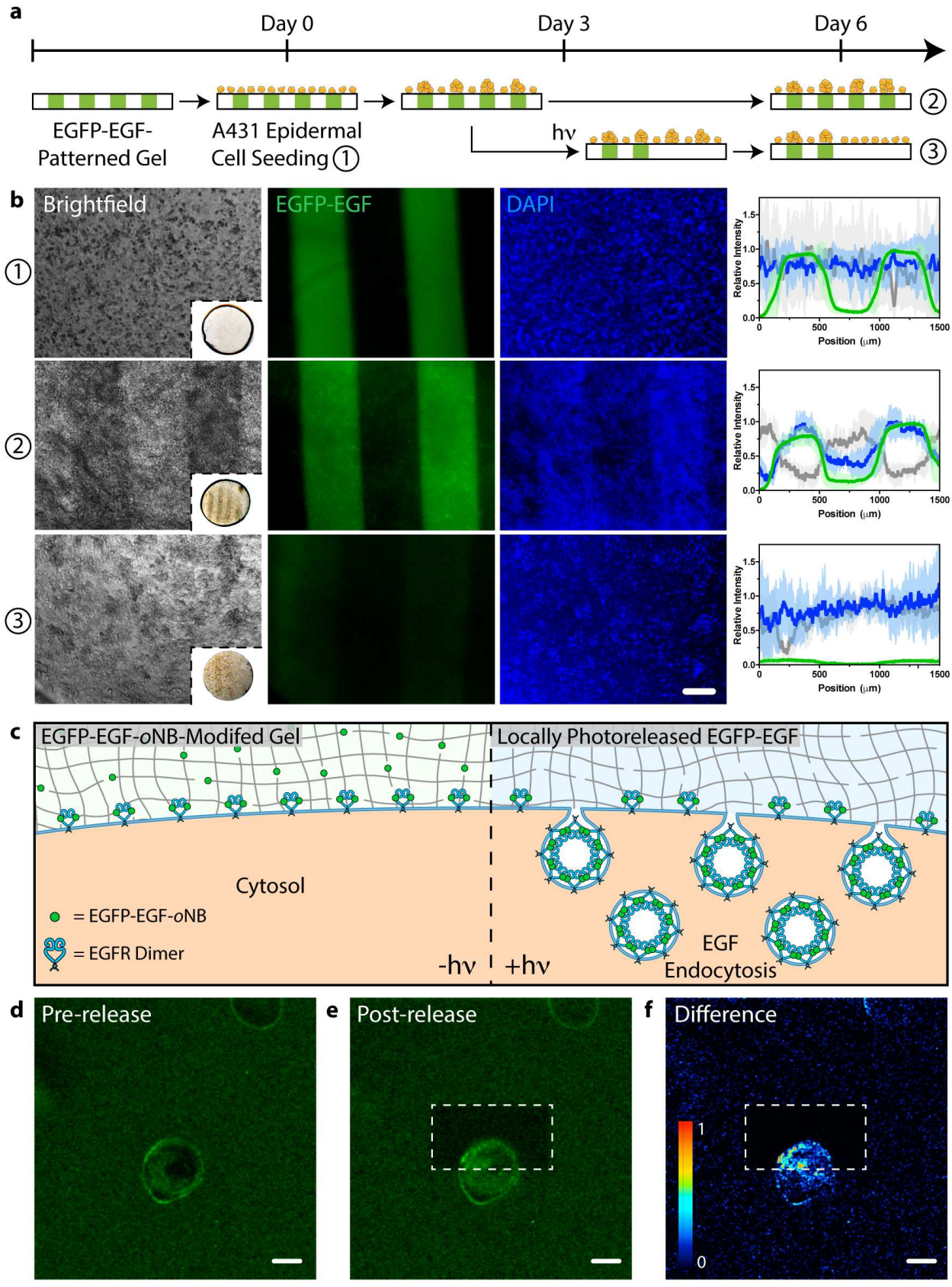
a
Day 0
Day 3
Day 6
EGFP-EGF-
Patterned Gel
A431 Epidermal
Cell Seeding ①
hν
②
③
b
Brightfield
EGFP-EGF
DAPI
①
②
③
Relative Intensity
Position (μm)
c
EGFP-EGF-oNB-Modifed Gel
Locally Photoreleased EGFP-EGF
Cytosol
= EGFP-EGF-oNB
= EGFR Dimer
-hν
+hν
EGF
Endocytosis
d
Pre-release
e
Post-release
f
Difference
1
0

Figure 6 | Modulating cell fate with a photoreleasable sortagged fluorophore-growth factor chimeric protein. a. Patterned population-level control of A431 cell proliferation is achieved through stimulation with gel-immobilized EGFP-EGF-*o*NB-N_3 in 2D culture. Protein photoremoval promotes dynamic cell redistribution. Key analytical timepoints are noted on the experimental timeline with circled numbers. **b.** Brightfield and fluorescent images highlight cell response (nuclei in blue) to patterned EGFP-EGF-*o*NB-N_3 (green) at various experimental endpoints. Relative intensity profiles are given for EGFP (green), nuclei (blue), and optical transmission (grey) across gels perpendicular to photopatterned lines, with average values (dark lines) and standard deviations (light error bars) corresponding to data from three biological replicates (n = 3). Brightfield insets depict full hydrogel (~0.5 cm in diameter). Images and analysis in condition ③ correspond to the gel half whose protein was photoreleased on Day 3. **c.** Encapsulated cells bind but cannot internalize hydrogel-tethered EGFP-EGF-*o*NB-N_3. Photoliberation of the soluble protein promotes canonical EGFR activation and associated membrane endocytosis. **d-e.** EGFP-EGF protein release is confined to gel subvolumes bisecting a single A431 cell in 3D culture. Endosome formation is visible in <5 minutes and concentrated in the regions of light exposure. Fluorescent images correspond to timepoints (**d**) immediately preceding and (**e**) 5 minutes after protein photorelease within a single gel. **f.** Difference calculations between images pre- and post-release highlight local EGFP-EGF internalization. Scale bar = 200 μm in **b** and 10 μm in **d-f**.